ANOMALOUS DIFFUSION IN A LINEAR PLASMA GENERATOR

O. WALDMANN[1], H. MEYER[2], AND G. FUSSMANN[3]

ABSTRACT. Plasma production and particle transport of the magnetized plasma in the linear device PSI-2 are investigated by analyzing the radial density and electron temperature profiles obtained from Langmuir probe measurements. Additional information on the atomic (H) and proton temperatures is obtained from high resolution Doppler spectroscopy. The density profiles are found to be hollow, but do extend radially far beyond the visible rim with an exponential decay length of 3 cm. They can be explained by parallel and perpendicular diffusion in combination with a cylindrical source extending along the magnetic field all over the device. A large perpendicular diffusion coefficient in the range of 5 m^2/s is inferred from the experimental results.

The definitive version is available at www3.interscience.wiley.com

1. INTRODUCTION

The transport of a fully ionized plasma across a strong magnetic field has been a subject of controversial discussion for a long time. Already in the early 50-ies of the last century one realized that coulomb collisions among the charged particles will cause a random walk of the electrons and ions because each collision is associated with a shift of the order of the Larmor radius (ρ). First theoretical treatments of the problem by Taylor [1] in 1961 revealed that this so called "classical diffusion" is characterized by a very small diffusion coefficient $D_\perp^{\mathrm{class}} = \rho_\mathrm{e}^2\ \nu_\mathrm{ei} \sim n_\mathrm{e} B^{-2}$ since only the rather ineffective electron-ion collisions contribute to the particle transport. Because of $\rho_\mathrm{e}^2\ \nu_\mathrm{ei} = \rho_\mathrm{i}^2\ \nu_\mathrm{ie}$ this diffusion coefficient is equal for electrons and ions, hence the transport is intrinsically ambipolar and no electric fields are needed to enforce a quasi neutral plasma flux.

During the following years questions came up with respect to the validity of classical diffusion since in the experiments generally much larger diffusion coefficients were found. Only the very quiescent Q-machines (see [2]) showed values compatible with $D_\perp^{\mathrm{class}} \approx 0.001 \ldots 0.01\ \mathrm{m}^2\mathrm{s}^{-1}$ but particularly toroidal devices like stellarators and tokamaks were characterized by dramatically larger values of typically $1\ \mathrm{m}^2\mathrm{s}^{-1}$. However, D. Pfirsch and A. Schlueter [3] noticed that in a torus a considerably enhanced transport is to be expected because of the curvature of the field lines. But even taking a corresponding factor of order 10 to 20 into account the experimental diffusion coefficients remained much larger than the predicted ones. L. Spitzer [4] seems to be the first who had the idea that fluctuating electric fields might be the reason for the – meanwhile called – "anomalous" transport. He derived an expression for the diffusion coefficient in which the magnetic field entered only via $1/B$, i.e. much weaker than in the classical case. D. Bohm fixed a pre-factor that had been left undefined by Spitzer to $1/16$ (without presenting the derivation) and came up with his famous formula $D_\perp^{\mathrm{Bohm}} = k_\mathrm{B} T/(16eB)$ that appeared to be in agreement with many observations (see e.g. [5]).

Anomalous plasma transport caused by turbulent electric fields is still a matter of actual research and a large number of theoretical and experimental papers is devoted to this topic

[1]Corresponding author: OWaldmann@lbl.gov

Key words and phrases. Transport properties, magnetized plasmas, probe measurements.

(see e.g. [6]-[9]). In what follows we want to add an experimental contribution based on observations made in the linear device described in the next section. For quite a while we were uncertain about the transport prevailing in this stationary plasma since the observations appeared to be contradictory. In fact, in 2000 we published a paper [10] claiming that classical diffusion is the prevailing transport in the device. This was inferred from the observation of hollow density profiles existing over a length of more than 2 m along the magnetic axis. The hollowness of the profiles demanded a diffusion coefficient of less than 0.04 m^{2}s^{-1}, being about the classical value. This assumption was corroborated by the observations of so called "plasma shadows" [11] that are produced when obstacles like probes are inserted into the plasma. A dark shadow extending over a length of 1 m or more with a surprising sharp contour is to be seen in the down stream direction. On the other hand, the walls of the cylindrical stainless vessel get astonishingly hot (50...80 C) during long term operation. This is difficult to explain invoking radiative heating alone. Moreover, the plasma edge produced by the limiting effect of the hollow anode does not show an abrupt decay as it were to be expected in case of a very small diffusion coefficient. In particular this latter inconsistency caused us to resume the studies on perpendicular transport. We will show that in contradiction to our earlier interpretation a consistent picture can be obtained when the plasma sources in the streaming region are taken carefully into account and anomalous diffusion is assumed.

From a principal point of view measurement of the diffusion coefficient is a straight forward matter. According to the definition of a diffusive flux $\vec{\Gamma} = -D\ \nabla n$ it should be determined from the ratio of the flux density and the density gradient. Clearly, the density gradient is not so much a problem but the flux density is difficult to measure. Most suitable are passive or active optical methods (LIF) relying on the Doppler effect. However, the associated velocity shift of the ion distribution $\langle v \rangle = D|\nabla n|/n$ is often too small to be detected. Apart from the fact that these direct methods fail in case of hydrogen plasmas treated in this study, they cannot be applied to PSI-2 plasmas because of the very small mean velocity which is estimated to be less than 1% of the thermal one.

One is therefore obliged to invoke another (indirect) method as it is for example enabled by the continuity equation. There is, however, the difficulty that under stationary conditions (our case) the information contained in the radial profiles of plasma density is insufficient to determine the perpendicular diffusion coefficient and particle sources as well as parallel transport must also be taken into account. It is an advantage that in the present situation the sources are confined to a thin cylindrical shell allowing an analytical treatment of the problem. It will be shown in Sec. 4.1 that without parallel transport (very long cylinders or tori) the radial profiles degenerate to a function that does not contain any information on the perpendicular diffusion coefficient. Nevertheless, $D_\perp$ can be obtained from the particle balance if the source strength is known. In sections 4.2 a and 4.2 b two different approaches are pursued to incorporate the parallel losses. They lead to very similar results Sec. 5). In both cases there are two different ways to determine $D_\perp$ from the particle balance: either by including the source region or by excluding it. In the latter case the perpendicular losses are balanced by the parallel ones ($\nabla_\perp \cdot \vec{\Gamma}_\perp + \nabla_\parallel \cdot \vec{\Gamma}_\parallel = 0$) and if the latter are known, the former, and thus $D_\perp$ can be determined.

A description of the apparatus and the main diagnostics is given in Sec. 2. Apart from the radial profiles of electron density and temperature (n_e, T_e) that are obtained from Langmuir probes additional information on the ion temperature and, most important, on the neutral density are needed. This experimental material – mainly delivered by spectroscopy – is

presented in Sec. 3. The results attained from the various methods and approximations are presented in Sec. 5. They are followed up by a short discussion given in the summary.

2. EXPERIMENTAL SET-UP

2.1. **Plasma generator PSI-2.** The plasma generator PSI-2 shown in Fig. 1 is a linear device showing cylindrical symmetry. The plasma is produced by an electrical current (typically 50 to 500 A) flowing between a heated hollow cathode (inner and outer diameters 6.0 and 7.0 cm, respectively) made from LaB_6 and a massive Mo anode 20 cm in length with a conical bore shrinking from 8 to 6 cm in diameter in the down stream direction. The anode is earthed whereas the potential of the cathode is typically between -50 to -100 V. The working gas, such as hydrogen or argon, is replenished from the cathode end. After ionization and heating a pressure gradient is built up that drives the produced plasma downstream toward the neutralizer plate. An axial magnetic field (B) confines the plasma radially. The radius of the visible plasma column is typically $r_{\text{plas}} \approx 5$ cm; it varies with the local magnetic field strength according to flux conservation, i.e. $B(z)r^2_{\text{plas}} = B(z_{\text{anode}})r^2_{\text{anode}}$. In a similar way we can also map the cathode along the field lines: $B(z_0)r_0^2 = B(z_{\text{cath}})r^2_{\text{cath}}$. It turns out that at the position of measurement (indicated in Fig. 1) the magnetic field strength is equal to the cathode value, thus, predicting $r_0 = r_{\text{cath}} = 3.0 \ldots 3.5$ cm. The experimentally observed value $r_0 = 3.5$ cm (see Fig. 5) appears hence to coincide with the outer radius of the cathode.

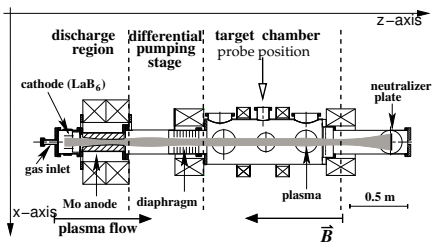

FIGURE 1. Plasma Generator PSI-2

I	200	A
B	0.1	T
$n_{\text{e}}(\text{max})$	$7 \cdot 10^{17}$	m^{-3}
$T_{\text{e}}(\text{max})$	11	eV
T_{i}	0.4	T_{e}
p_{H_2}	0.050	Pa
T_{H}	1800	K

FIGURE 2. Plasma parameters in the target chamber

After leaving the anode the plasma streams through a differential pumping stage into the target chamber and towards a neutralizer plate made from Mo. The target chamber is separated from the pumping stage by diaphragms to reduce the neutral pressure in the rear part of the device. The chamber extends over a length of 1.5 m and its radius ($r_{\text{w}} = 20$ cm) is large to reduce the plasma interaction with the wall of the vessel to a very low level. In a distance of 2.6 m from the cathode the plasma hits the neutralizer plate where it finally recombines and the neutral gas is pumped away. Usually the neutralizer plate is kept at floating potential. Under these (normal) conditions the whole region between anode and neutralizer target is free of electrical current.

Because of the ring shaped discharge region in the vicinity of the cathode the plasma shows generally hollow profiles in electron temperature and density (cf. Fig. 5) all along the magnetic axis. Only in case of very high densities ($n_{\text{e}} \geq 3 \cdot 10^{19}\text{m}^{-3}$) flat or peaked profiles are found in the target region.

Some characteristic parameters are collated in Table 2. $p_{\text{H}_2} = 0.05$ Pa is the pressure

of the molecules as measured by a "viscovac" pressure meter in a dead end duct about 1 m away from the plasma where the temperature is around 30 °C, i.e. $T_{H_2} = 300$ K. From the ideal gas law $p_{H_2} = n_{H_2} k_B T_{H_2}$ we obtain the molecular density to $n_{H_2} = 1.2 \cdot 10^{19}$ m^{-3}. A crucial quantity is the temperature of the neutral atoms in the plasma region. First measurements using thin, shielded thermocouples yielded temperatures around 800 K. However, because of radiation and heat conduction losses they tend to underestimate the temperature considerably and large corrections are necessary. We therefore rather rely on the spectroscopically determined value $T_H \approx 1800$ K described in Sec. 3.
For the plasma region the ionization and dissociation lengths are estimated at $\lambda_{ion} = 2.4$ m and $\lambda_{diss} = 0.16$ m, respectively. Hence, the molecules are likely to be disintegrated to atoms within a few passages through the plasma whereas the atoms have a much longer life time and therefore do occur with about ten times higher abundance. They build up an almost homogeneous density that can be estimated assuming pressure equilibrium of the neutrals between duct and target chamber. Neglecting the molecules in the latter we get $n_H = n_{H_2} \cdot (T_{H_2}/T_H) = 2 \cdot 10^{18}$ m^{-3}.

2.2. **Langmuir probes.** Single probe measurements [12] with two Langmuir probe tips of different dimensions (small: diameter $d = 1.5$ mm, height $h = 1.5$ mm; large: $d = 8$ mm, $h = 8$ mm) have been performed. Because of the proportionality of the ion saturation current to the collecting area of the probe tip, the sensitivity of the measurement is determined by the size of the probe tip. A large probe tip is suited for a region of low electron temperature and density but the energy picked up by the probe in a region of higher density and temperature can easily be too large and cause melting. For this reason the two probes described above were used for the outer and inner plasma regions with an overlap zone of about 1 cm in radial direction. The application of the large probes in the outer plasma region is actually an essential improvement. They eliminate the preliminary uncertainty with respect to the true decay lengths in the wings. In fact, it is found that the smaller probes have the tendency to overestimate the density considerably if $n_e < 10^{17}$m^{-3}.
The I-U characteristics of the single probes are evaluated applying Langmuir probe theory for a collisionless regime (see [13] and references therein). The electron density is evaluated from the ion saturation current. Since the ion gyro-radius is larger than the probe diameter – and besides the ions are hardly magnetized – the total tip surface $A_i = \pi dh + \pi d^2/4$ is taken as collecting area. The electron temperature is determined from the exponential slope of the current at floating potential. In addition $T_i \approx 0.5\ T_e$ can be assumed as explained in Sec. 3.1 and in [14]. The currents do show well defined ion saturation levels; no indications for deviations from Maxwellians are to be inferred from the characteristics. The radial movement, the applied voltage and the measurement of the current of the Langmuir probes are computer controlled. Thus complete radial profiles with good spatial resolution can be measured.

3. Experimental data

3.1. **Measurement of the proton temperature.** Information on the ion temperature can often be obtained from Doppler broadening of some suited emission line. In case of hydrogen, however, it is generally believed that this method fails because there is no line emission from the protons. Nevertheless, we found the method applicable due to the charge exchange effect. To explain the method we refer to Fig. 3 which shows a spectrum of H_α recorded with a 3 m spectrometer providing a resolution as high as $\lambda/\Delta\lambda \approx 10^5$. As to be seen, the spectrum is not symmetric with respect to the maximum of intensity but shows a shoulder on its red wing. It is important to note that the spectrum was taken along a chord

of sight in the upper halve of the plasma column. In fact, changing to a chord in the bottom region the shoulder appears on the blue wing of the spectrum and it disappears along a central chord. Moreover, changing the direction of the magnetic field causes the spectral asymmetry to invert sign too. The shoulders are therefore associated with the rotation of the protons (see [15] for further information).

The spectroscopic shift is provided by excited H atoms that just have been generated from

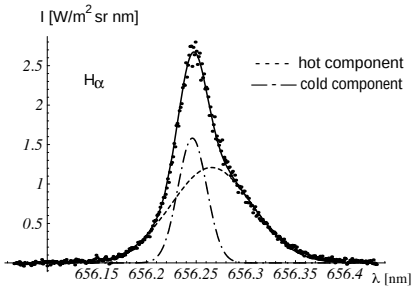

FIGURE 3. Measured line profile of H_α in high resolution showing cold and hot components due to dissociation and charge exchange, respectively.

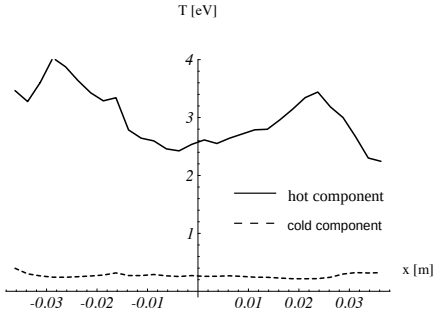

FIGURE 4. Profile of the proton temperature (solid line) over the central plasma cross-section.

the protons by charge exchange and therefore still reflect their motion. As indicated in Fig. 3 it is possible to decompose the spectra in a cold, unshifted component and a shifted hot one. The cold component is representative of such H atoms that have been produced by dissociation and left excited in the $n = 3$ state. As shown in Fig. 4 their temperature is about 0.16 eV ≈ 1800 K. Of equal interest is the hot component that delivers information on the plasma rotation velocity and the proton temperature. The shift $\Delta\lambda_{\rm s} = 0.002$ nm and half-width $\Delta\lambda_{1/2} = 0.035$ nm taken from Fig. 3, for instance, correspond to $v_{\rm rot} = 915$ m/s and $T_{\rm i} = 3.9$ eV.

The above method has been applied to space resolved measurements. After Abel inversion [16] the proton temperature profile shown in Fig. 4 could be reconstructed from the measurements.

$T_{\rm i}$ is seen to be about 2.5 to 4 eV in the core region $r < 3.5$ cm which is about 40% of the electron temperature. Unfortunately, intensity problems do not allow to extend the measurement to the outer plasma regions. It is worth to mention that these results are supported by laser induced fluorescence (LIF) measurements performed in argon. From these we learnt that the ion temperature is typically about $1/2$ of the electron temperature [14].

3.2. **Density profiles.** The hollow profile within and the slow decay of density outside of the visible plasma column ($r \approx 5$ cm) can be clearly seen in Fig. 5 representing a measurement in hydrogen ($I = 200$ A). The black area in Fig. 5 is the projection of the cathode.

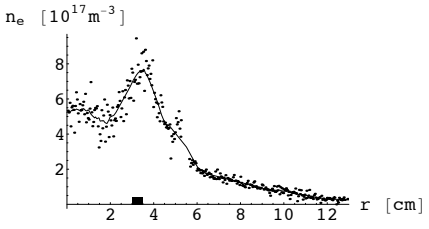

FIGURE 5. n_e-profile of a hydrogen plasma measured with two Langmuir probes (Data points and fitting curve). The black area marks the projection of the cathode.

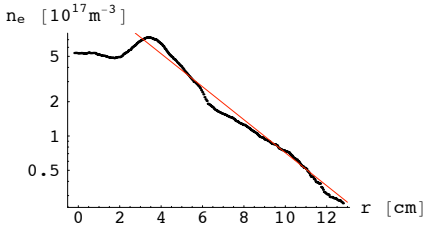

FIGURE 6. Log-linear-plot of n_e-profile in comparison with the exponential $n_e \propto \exp(-r/\lambda)$ with $\lambda = 3$ cm.

Actually, in Fig. 5 only the data for $x \leq 0$ are shown where x is the direction from top to bottom. Data with $x \geq 0$ are ignored because at these positions the probe shaft is increasingly perturbing the measurement due to cooling of the corresponding magnetic surface. In Fig. 6 the experimental profile is again presented but this time on a logarithmic scale to visualize the slow exponential decay in the outer region. In fact, the density in the region $r \geq 3.5$ cm decays exponentially with a characteristic decay length of $\lambda = 3.0$ cm. At a radius of $r = 10.5$ cm the density is still about 10% of the maximum value at $r = 3.5$ cm. The "hollowness" expressed by the ratio of maximum density ($7 \cdot 10^{17}$ m^{-3}) and core value $n_e(0)$ is approximately 7:5.
Actually the density shows three regions of exponential decay outside $r = 4$ cm, which are not fully understood yet (see Fig. 6). The first ($r = 4 \ldots 6$ cm) and the third ($r = 10 \ldots 12$ cm) region have the same decay length, while the second one ($r = 6 \ldots 10$ cm) has a shorter one. However, the theory presented in the following sections aims to explain the general trend rather than the fine structure of the profile.

4. THEORY: DIFFUSION PROFILES IN CASE OF AN EXTENDED PLASMA SOURCE

In what follows we will assume that the hot electrons leaving the cathode region establish a source all along the device. Although there is no doubt that the plasma production rate in the discharge region is much higher than in the remaining part of the device one has to take into account that a major fraction of the primary produced plasma is lost by recombination at the anode surface. On the other hand, the energy flux due to parallel electron heat conductivity into the current free region is regarded as essential. It is this heat flux which provides a rather high electron temperature (enabling ionization) on the magnetic surface being in contact with the cathode. The importance of this source term will be verified in the following section.

4.1. **Cylindrical source of infinite length.**

It is instructive to consider first a source consisting of a thin cylinder $r_0 - \Delta/2 \leq r_0 \leq r_0 + \Delta/2$ of infinite length. The equation of

continuity then reads

$$\frac{\partial n_\mathrm{e}}{\partial t} = \frac{1}{r}\frac{\partial}{\partial r} r D_\perp \frac{\partial n_\mathrm{e}}{\partial r} + q = 0\,, \tag{1}$$

where the source strength $q = n_\mathrm{e} n_\mathrm{H} \langle \sigma_\mathrm{ion} v_\mathrm{e} \rangle = n_\mathrm{e} \nu_\mathrm{ion}$ is determined by ionization. The ionization frequency ν_ion is given by the product of the neutral density n_H and the ionization rate coefficient $S(T_\mathrm{e}) = \langle \sigma_\mathrm{ion} v_\mathrm{e} \rangle$ which is a monotonously rising function of the electron temperature. Per unit length and time the source produces

$$\dot{N}_\mathrm{e} = \int_0^\infty q\, 2\pi r\, dr = n_\mathrm{e}(r_0)\nu_\mathrm{ion}(r_0) 2\pi r_0 \Delta \tag{2}$$

electrons and ions. In Fig. 7 the measured profiles of T_e and the ionization source strength q are shown, using either [17] or the simple formula given in [18] to calculate the ionization rate coefficient for hydrogen. We see that the latter is approximately a Gaussian centered at $r_0 = 3.5$ cm with full half width $\Delta = 2$ cm. With $T_\mathrm{e}(r_0) \approx 11$ eV and $n_\mathrm{H} \approx 2 \cdot 10^{18}$ m^{-3} we estimate $\nu_\mathrm{ion}(r_0) = 1.4 \cdot 10^4$ s^{-1} and inserting this into Eq. (2) we get $\dot{N}_\mathrm{e} = 0.44 \cdot 10^{20}$ m^{-1}s^{-1}.

We are now also in the position to assess the importance of the source term. We can do this by multiplying the ratio $\dot{N}_\mathrm{e}/N_\mathrm{e} = \nu_\mathrm{ion}$ by the residence time which later will be estimated at $\tau = 0.26$ ms. The result $\nu_\mathrm{ion}\tau = 4$ tells us that the number of electrons and ions entering the current free region via the anode will be amplified by this factor due to ionization.

For convenience we want to simplify the source function even further by replacing it by a Dirac function: $q = n_\mathrm{e}(r_0)\nu_\mathrm{ion}(r_0)\Delta\ \delta(r - r_0)$. Inserting this into Eq. (1) and assuming

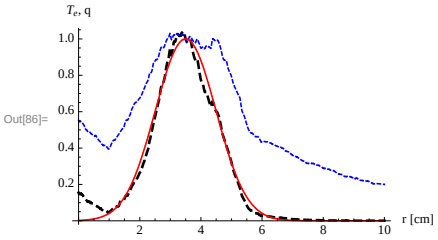

FIGURE 7. Normalized radial profiles of electron temperature (blue, dotted, $T_\mathrm{e,max} = 11$ eV), source strength $\hat{q} \propto n_\mathrm{e}\ S_\mathrm{ion}(T_\mathrm{e})$ (black, solid, $S_\mathrm{max} = 7 \cdot 10^{-15}$ m^{3}s^{-1}) and its approximation $\hat{q} = \exp\left(-((r-3.5)/1.4)^2\right)$ (red, dashed).

$D_\perp$ = const. Its solution is obtained by integration to

$$n_\mathrm{e} = \begin{cases} n_\mathrm{e}(0) & r \le r_0 \\ n_\mathrm{e}(0) - \frac{\dot{N}_\mathrm{e}}{2\pi D_\perp} \ln\left(\frac{r}{r_0}\right) & r > r_0 \end{cases}. \tag{3}$$

Because $\ln r$ rises monotonously, n_e will become negative beyond a certain radius which, of course, is not acceptable from a physical point of view. It actually means that a stationary solution is not possible without an absorbing wall. We will assume that such a wall enforces

the density to vanish at radius r_w [1]. Then Eq. (3) becomes

$$n_\mathrm{e} = n_\mathrm{e}(0) \begin{cases} 1 & r \le r_0 \\ 1 - \frac{\ln(r/r_0)}{\ln(r_\mathrm{w}/r_0)} & r_0 < r \le r_\mathrm{w} \end{cases} . \tag{4}$$

Under stationary conditions the total flux leaving the source region

$$\Phi = -2\pi r_0 D_\perp \frac{dn_\mathrm{e}}{dr}|_{r=r_0} = 2\pi D_\perp \, n_\mathrm{e}(0)/\ln(r_\mathrm{w}/r_0) \tag{5}$$

must equal the production rate $\dot{N}_\mathrm{e}$ given by Eq. (2). Because of $n_\mathrm{e}(r_0) = n_\mathrm{e}(0)$ the density at source radius cancels and the balance reads

$$D_\perp = \nu_\mathrm{ion}(r_0) \, r_0 \, \Delta \ln(r_\mathrm{w}/r_0) \, , \tag{6}$$

which alternatively may be derived by equalizing the second lines in Eqs. (3) and (4). Inserting the values already given we get $D_\perp = 17.2$ m^2/s. If the profile given by Eq. (4) would fit to the measurements we would thus have determined the diffusion coefficient though this quantity does not explicitly appear in the solution for the n_e profile. Let us check whether this solution complies with our measurements. With the radii $r_0 = 3.5$ cm and $r_\mathrm{w} = 20$ cm for source and wall we get for the ratio $n_\mathrm{e}(3r_0)/n_\mathrm{e}(r_0) = 1 - \ln(3)/\ln(20/3.5) = 0.37$ which is by a factor 3.7 too large compared to the measured ratio of 0.1. Parallel particle losses along the field lines are therefore to be included which will result in a faster decay of the density profile.

The question remains: what does actually determine the density at the source radius $n_\mathrm{e}(r_0)$? The answer is hidden in the energy equation. While the major part of the input power P is lost at the anode and transferred to the neutralizer plate by electron heat conduction only a small fraction of about $\eta = 5 - 10\%$ is available for ionization, excitation and heating in the target chamber $P_{ion} = \eta P = L_\mathrm{cham} \dot{N}_\mathrm{e} \bar{E}$ with $\bar{E} = E_\mathrm{ion} + E_{exc} + 5/2(kT_\mathrm{e} + kT_\mathrm{i})$. Because of $\dot{N}_\mathrm{e} \propto n_\mathrm{e}(r_0)\nu_{ion}(r_0)$ we may write $P = c_1 n_\mathrm{e}(r_0)\nu_{ion}(r_0)$ where c_1 is a constant. From the particle balance Eq. (6) we have on the other hand $\nu_{ion} = c_2 D_\perp$, where c_2 is another constant containing the slope of the n_e-profile at $r = r_0$. It then follows $n_\mathrm{e}(r_0) = P/(c_1 c_2 D_\perp)$.

4.2. **Diffusion with source and loss terms.** In the last section it was shown that the assumption of pure radial diffusion does not lead to a density profiles consistent with the observation. It is therefore necessary to consider the particle losses parallel to the field lines too. We will consider two different approximations to take these losses into account. The first approach is to replace the corresponding term -$\partial_z \Gamma_\parallel$ by a loss term $-\nu_\mathrm{loss} n_\mathrm{e}$. This simple approach is widely used to treat particle transport in the scrape-off region of fusion devices (see e.g. [20]). In the second case the parallel flux density $\Gamma_\parallel = u_\parallel n_\mathrm{e}$ is converted into a diffusive term $-D_\parallel \partial_z n_\mathrm{e}$ which is shown to be possible if the temperature along the field lines is constant. This invariance of the axial temperature was substantiated by means of probe measurements [12] and is confirmed by numerical code calculations [21].

a) Loss frequency concept

This concept appears particularly reasonable when the mean free path length of the ions due to momentum transfer collisions with the neutrals

$$\lambda_\mathrm{i} \approx \frac{\overline{v}_\mathrm{i}}{n_\mathrm{H} \langle \sigma_{\mathrm{i}0}^\mathrm{cx} v_\mathrm{i} \rangle} \approx (n_\mathrm{H} \sigma_{\mathrm{i}0}^\mathrm{cx})^{-1} \tag{7}$$

[1]The situation is similar to a capacitor consisting of two concentric infinite cylinders. Its capacitance per unit length $C = 2\pi\epsilon/\ln(r_w/r_0)$ vanishes for $r_w \to \infty$ (see [19] for a discussion).

is much longer than the length of the plasma. Here $\bar{v}_\mathrm{i} = \sqrt{\frac{8k_\mathrm{B}T_\mathrm{i}}{\pi m_\mathrm{i}}}$ is the mean velocity of the ions and only the dominating charge exchange collisions have been considered. The stationary equation of continuity then reads:

$$0 = \frac{1}{r}\frac{\partial}{\partial r} r D_\perp \frac{\partial n_\mathrm{e}}{\partial r} + (\nu_\mathrm{ion} - \nu_\mathrm{loss})\, n_\mathrm{e}\ . \tag{8}$$

The frequency of the losses is obtained by distributing the ion losses at the neutralizer plate over the volume. This leads to $\nu_\mathrm{loss} = 1/\tau_\parallel = \Gamma_s\ dA/(n_\mathrm{e} L\ dA)$. Note that the infinitesimal area $dA = 2\pi r\ dr$ cancels. Here, Γ_s, the particle flux density at the target surface, equals the ion saturation flux density $\Gamma_\mathrm{s} = 0.5\ n_\mathrm{e} c_\mathrm{i}$. Inserting for c_i the ion sound velocity we finally get

$$\nu_\mathrm{loss} = \frac{1}{2L}\sqrt{\frac{k_\mathrm{B}(T_\mathrm{e} + T_\mathrm{i})}{m_\mathrm{i}}}\ . \tag{9}$$

Again, Eq. (8) will not allow us to determine the absolute value of the electron density but only its shape. This is because the (anomalous) diffusion coefficient $D_\perp$ and the ionization and loss frequencies do not depend on n_e. Having thus found a particular solution of Eq. (8), then multiplying this function by a constant factor will again be a solution. As indicated in the last subsection the absolute density can be obtained only by invoking the energy equation.

We want to solve Eq. (8) by first approximating the source term by a δ-function and assuming $D_\perp$ and ν_loss being constants. We then get the equation

$$\frac{1}{r}\frac{\partial}{\partial r} r \frac{\partial n_\mathrm{e}}{\partial r} - k^2 n_\mathrm{e} = -\frac{\nu_{ion} n_\mathrm{e} \Delta}{D_\perp}\delta(r - r_0) \tag{10}$$

with $k = \sqrt{\nu_\mathrm{loss}/D_\perp}$. Eq. (10) is solved by the modified Bessel functions I_0(r) and K_0(r) that satisfy the following relations for $x \ll 1$: $I_0(x) = 1, K_0(x) = -\ln(x/2) + 0.577\ldots$, and for $x \gg 1$: $I_0(x) = \frac{1}{\sqrt{2\pi x}}\exp(x)$, $K_0(x) = \sqrt{\frac{\pi}{2x}}\exp(-x)$. Assuming the absorbing wall at infinity the solution is therewith obtained to

$$n_\mathrm{e}(r) = A \begin{cases} I_0(kr)K_0(kr_0) & r \le r_0 \\ I_0(kr_0)K_0(kr) & r \ge r_0 \end{cases}. \tag{11}$$

Integrating Eq. (10) over the infinitesimal range $r_0 - \epsilon \le r \le r_0 + \epsilon$ and applying the Wronski relation $K_0'(x)I_0(x) - K_0(x)I_0'(0) = -1/x$ the coefficient is found to be

$$A = \nu_{ion}(r_0)\ n_\mathrm{e}(r_0)\ r_0\ \Delta/D_\perp. \tag{12}$$

Inserting this into in Eq.(11) and putting $r = r_0$ the density at the source region cancels and we get a relation for the diffusion coefficient similar to Eq. (6)

$$D_\perp = \nu_\mathrm{ion}(r_0)\ r_0\ \Delta\ I_0(kr_0)K_0(kr_0)\ . \tag{13}$$

With the same data as before and anticipating $k = 33\ \mathrm{m}^{-1}$ we get this time with $x_0 = kr_0 = 1.15$ and $I_0(x_0)\ K(x_0) = 0.46$ for the diffusion coefficient $D_\perp = 3.2{\cdot}10^{-4}\ \nu_{ion} = 4.5\ \mathrm{m}^2\ \mathrm{s}^{-1}$. The more general treatment, including the true sources shown in Fig. 7, is presented in the appendix A. It will be shown there that the approximation (13) is a very good one.

By means of Eq. (12) and (13) the expression (11) can finally written as

$$n_\mathrm{e}(r) = n_\mathrm{e}(r_0) \begin{cases} I_0(kr)/I_0(kr_0) & r \le r_0 \\ K_0(kr)/K_0(kr_0) & r > r_0 \end{cases}. \tag{14}$$

This function is continuous at the position of the source r_0 but not so its derivative. It also shows the desired property of hollowness. Fitting this function to the measured profile will deliver a value of k from which in turn the diffusion coefficient can be obtained via

$$D_\perp^{(a)} = \nu_{\text{loss}}/k^2 \ . \tag{15}$$

Whereas Eq. (13) results from the balance between source strength and fluxes this second relation follows from the balance of perpendicular and parallel losses in the source free region.

b) Parallel diffusion losses

Let us consider the parallel components of the momentum equations for electrons and ions:

$$\begin{aligned} 0 &= -\frac{\partial p_\text{e}}{\partial z} - e n_\text{e} E_z \\ 0 &= -\frac{\partial p_\text{i}}{\partial z} + e n_\text{i} E_z - m_\text{i} \nu_\text{m} n_\text{i} u_\parallel \end{aligned} \tag{16}$$

in which $\nu_\text{m} = \nu_{\text{i}0}^{\text{el}} + \nu_{\text{i}0}^{\text{cx}} + \nu_{\text{ion}}$ is the total momentum transfer frequency of the ions due to elastic and charge exchange collisions with the neutrals and production of ions by ionization, respectively. Because of their small mass a corresponding loss term can be neglected in case of the electrons. In addition, the inertia forces are neglected because of the damped motion enforced by the friction forces. Adding both equations in (16), assuming quasi-neutrality $n_\text{e} = n_\text{i} = n$ and constant temperatures, the electric field cancels and we get $k_\text{B}(T_\text{e} + T_\text{i})\, \partial_z n = -m_\text{i} \nu_\text{m} \Gamma_\parallel$. The ambipolar flux density is thus obtained to $\Gamma_\parallel = -D_\parallel \frac{\partial n}{\partial z}$ with

$$\begin{aligned} D_\parallel &= \frac{k_\text{B}(T_\text{i}+T_\text{e})}{m_\text{i}\ \nu_\text{m}} \\ &= \frac{k_\text{B}(T_\text{i}+T_\text{e})}{m_\text{i} n_\text{H} \langle (\sigma_{\text{i}0}^{\text{el}} + \sigma_{\text{i}0}^{\text{cx}}) v_\text{i} \rangle + \langle \sigma_\text{ion} v_\text{e} \rangle)} \ . \end{aligned} \tag{17}$$

In case of hydrogen charge exchange collisions are much more frequent than ionization and elastic collisions and the above expression simplifies to

$$D_\parallel = \lambda_\text{i} \sqrt{\frac{\pi\ k_\text{B} T_\text{i}}{8 m_\text{i}}} \left(1 + \frac{T_\text{e}}{T_\text{i}}\right) \tag{18}$$

with the mean free path length given by Eq. (7). The equation of continuity is this time given by

$$0 = \frac{1}{r}\frac{\partial}{\partial r} r D_\perp \frac{\partial n_\text{e}}{\partial r} + \frac{\partial}{\partial z} D_\parallel \frac{\partial n_\text{e}}{\partial z} + \nu_\text{ion} n_\text{e} \ . \tag{19}$$

Assuming constant diffusion coefficients and approximating the source term again by a δ-function its solution is found to be

$$\begin{aligned} n_\text{e}(r,z) = n_\text{e}(r_0) \cos(k_\parallel z) \times \\ \begin{cases} I_0(k_\perp r)/I_0(k_\perp r_0) & r \le r_0 \\ K_0(k_\perp r)/K_0(k_\perp r_0) & r > r_0 \ , \end{cases} \end{aligned} \tag{20}$$

whose radial part is the same as in the previous section, Eq. (14). The parameter $k_\perp$ is equivalent with the former k, but $k_\parallel$ is a new inverse length. The quantities are interlinked by

$$k_\perp^2 D_\perp = k_\parallel^2 D_\parallel \ . \tag{21}$$

which actually reflects the relation $\nabla_\perp \cdot \Gamma_\perp + \nabla_\parallel \cdot \Gamma_\parallel = 0$. Let us compare this relation with the one derived in the previous section Eq. (15). Denoting the present solution as $D_\perp^{(b)}$ we get for the ratio

$$\frac{D_\perp^{(b)}}{D_\perp^{(a)}} = D_\parallel \frac{2Lk_\parallel^2}{c_\mathrm{s}} \approx \frac{\pi^{5/2}}{9\sqrt{2}} \sqrt{1 + \frac{T_\mathrm{e}}{T_\mathrm{i}}}\, \frac{\lambda_\mathrm{i}}{L} = 2.4 \frac{\lambda_\mathrm{i}}{L} \,. \tag{22}$$

Here the approximate boundary condition $n_\mathrm{e}(L) = n_\mathrm{e}(0)/2$, leading to $k_\parallel = \pi/3L$, has been applied. With $\lambda_\mathrm{i} \approx 1$ m and $L = 2.6$ m the above ratio is about unity.
More accurately, the parameter $k_\parallel$ is defined by postulating the Bohm condition $u_\parallel = c_\mathrm{s}$ at $z = L$. The flow velocity is found from $u_\parallel = -D_\parallel \partial_z (\ln n_\mathrm{e})$ to be

$$u_\parallel = D_\parallel k_\parallel \tan(k_\parallel z) \,. \tag{23}$$

Multiplying by L and introducing $\zeta = k_\parallel L$ as a new variable, we have to solve the transcendental equation

$$a\,\zeta = \cot\zeta \qquad \text{with} \qquad a = \frac{D_\parallel}{L c_\mathrm{s}} \tag{24}$$

for ζ. Using this parameter, Eq. (21) may be written in the alternative form

$$D_\perp^{(b)} = \frac{c_\mathrm{s}}{L\, k_\perp^2} \zeta \cot\zeta = 2 D_\perp^{(a)} \zeta \cot\zeta \,. \tag{25}$$

The function $f(\zeta) = \zeta \cot\zeta$ (satisfying $f(0) = 1$ and $f(\pi/2) = 0$) provides a monotonous reduction with increasing ζ. Eq. (21) is thus the generalization of Eq. (13) when the interaction with the neutrals is to be taken into account.
Expression (23) allows us also to estimate the residence time of the particles starting at position z: $\tau(z) = \int_z^L u_\parallel^{-1}\, \mathrm{d}z$. In terms of ζ the result reads

$$\tau(z) = \frac{L^2}{D_\parallel}\, \zeta^{-2} \ln\left(\frac{\sin(\zeta)}{\sin(\zeta z/L)}\right) . \tag{26}$$

5. RESULTS

Fitting the experimental density profile shown in Fig. 6 by the analytical expression Eq. (20) a value of $k_\perp$= 33 m^{-1} is obtained. As to be seen from Fig. 8 the measurements are very well reproduced by the theoretical expression derived for the δ-like source function and an inclusion of the true source distribution does not lead to an essential improvement.
Having determined the value of $k_\perp$ we next estimate the mean free path length from Eq.

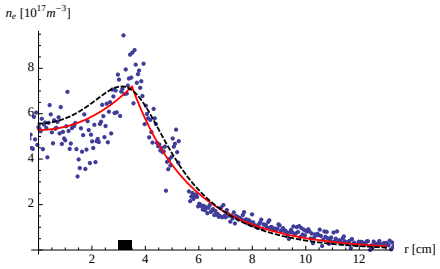

FIGURE 8. Comparison of measured (points) and theoretical n_e- profiles. Theory for a δ-source Eq. (14) (solid, red) and an extended source region Eq. (31) (dashed, black) are shown. The projection of the hollow cathode is indicated by a black box on the abscissa.

(7) neglecting the elastic collisions. With $n_{\rm H} = 2 \cdot 10^{18}$ m^{-3} and $\sigma_{\rm cx} \approx 5.0 \cdot 10^{-19}$ m^2 (see [22]) we find $\lambda_{\rm i} = 1.0$ m. Since this length is smaller than $L = 2.6$ m, the length of the device, we refer to Eq. (21) to calculate the perpendicular diffusion coefficient. As temperatures we insert the mean values $T_{\rm e} = 5$ eV, $T_{\rm i} = 3$ eV and obtain from Eq. (18) $D_\parallel = 28500$ m^{2}s^{-1} and $c_{\rm s} = 2.8 \cdot 10^4$ m/s. The parameter ζ is determined from Eq. (24) to 1.15 which results in a reduction factor of $f(\zeta) = 0.52$. $k_\parallel = \zeta/L$ is obtained to 0.44 m^{-1}. The flow velocity at the position of probe measurements is calculated from Eq. (23) to 5950 m/s corresponding to a Mach number of $M = u_\parallel/c_{\rm s} = 0.21$. The residence time for particles leaving the anode is estimated from Eq. (26) to $\tau = 0.26$ ms.
Finally, the desired perpendicular diffusion coefficient is received from Eq. (21) to $D_\perp = 5.1$ m^{2}s^{-1}. Almost the same values are obtained using the loss concept, Eq. (15) ($D_\perp = 4.9$ m^{2}s^{-1}), and from the different approach using the source strength, Eq. (13) ($D_\perp = 4.5$ m^{2}s^{-1}). These values are about twice the Bohm value $D_{\rm Bohm} = \frac{k_{\rm B}(T_{\rm e}+T_{\rm i})/2}{16eB} = 2.5$ m^{2}s^{-1}.
It should be noticed that the neutral density $n_{\rm H}$ enters the results differently. Whereas in the first two cases we have $D_\perp \propto D_\parallel^{-1} \propto 1/n_{\rm H}$ the perpendicular diffusion coefficient is proportional to the ionization frequency and thus $D_\perp \propto n_{\rm H}$ in the third case.

6. SUMMARY

The hollow plasma profile in PSI-2 has been diagnosed by means of Langmuir probes. It is found that the plasma extends radially far beyond the visible edge where it decays exponentially with a characteristic length of 3 cm. The measured profile can be well described by a theoretical function obtained by taking into account that there is a cylindrical particle source all over the length of the device. The transport is provided by anisotropic parallel and perpendicular diffusion.
Most important is the fact that the perpendicular diffusion coefficient determined is about two orders of magnitude larger than predicted by classical diffusion. With $D_\perp \approx 5$ m^{2}s^{-1} it is in the range of anomalous diffusion found in fusion devices although the plasma parameters ($n_{\rm e}$, $T_{\rm e}$, $T_{\rm i}$) and the magnetic field strengths in those are substantially larger. It should also be realized that in contrast to tokamaks or stellarators there is no curvature of the field lines in PSI-2. It thus appears that magnetically confined plasmas are driven – probably by turbulent mechanisms – in such a way that $D_\perp$ is always in the range of a few m^{2}s^{-1}. We therefore would like to encourage those who are developing turbulent transport codes to use the information given in this paper for benchmarking their theories.

APPENDIX A. RADIAL PROFILES

Solution (11), obtained for a δ- source function, allows us to calculate the density function for any source distribution $q(r) = n_0\, n_{\rm e} S_{\rm ion}$ by integration:

$$n_{\rm e}(r) = \frac{1}{D_\perp}\left(I_0(kr)\int_r^\infty K_0(kr')\, q(r')\, r'\, dr' + K_0(kr)\int_0^r I_0(kr')\, q(r') r'\, dr' \right) . \tag{27}$$

Introducing the normalized source function by means of $\hat{q} = q(r)/q_{max}$ with $q_{max} = \nu_{ion}(r_0)\, n_{\rm e}(r_0)$ and the dimensionless radial coordinate x = k r we have the general result

$$n_{\rm e}(x) = n_{\rm e}(x_0)\frac{\nu_{ion}(x_0)}{k^2 D_\perp}\left(I_0(x)\int_x^\infty K_0(x')\hat{q}(x')\, x'\, dx' + K_0(x)\int_0^x I_0(x')\hat{q}(x') x'\, dx' \right) . \tag{28}$$

Putting $x = x_0$, we get an identity from which the general relation

$$D_\perp = \frac{\nu_{ion}(x_0)}{k^2} \left(I_0(x_0) \int_{x_0}^{\infty} K_0(x')\hat{q}(x')\, x'\, dx' + K_0(x_0) \int_0^{x_0} I_0(x')\hat{q}(x')x'\, dx' \right) . \tag{29}$$

is received. With the source function shown in Fig. 7 a value of $D_\perp = 3.0{\cdot}10^{-4}\, \nu_{ion}(r_0) = 4.5$ m ^{2} s $^{-1}$ is obtained by numerical integration – in good agreement with the first approximation derived from Eq.(13).

Note that $x_0 = kr_0$ is the radius where the derivative of the source function vanishes $dq/dx|_{x_0} = 0$. This does in general not coincide with the maximum of n_e. This position is obtained from $dn_\mathrm{e}(x)/dx|_{x=x_m} = 0$. Inserting Eq. (28) it is found by solving the transcendent equation

$$I_1(x_m) \int_{x_m}^{\infty} K_0(x')q(x')\, x'\, dx' = K_1(x_m) \int_0^{x_m} I_0(x')q(x')x'\, dx' . \tag{30}$$

Having determined this position, the normalized profile $\hat{n}(x) = n_\mathrm{e}(x)/n_\mathrm{e}(x_m)$ is given by

$$\hat{n}(x) = \frac{I_0(x) \int_x^{\infty} K_0(x')\, q(x')\, x'\, dx' + K_0(x) \int_0^{x} I_0(x')\, q(x')x'\, dx'}{I_0(x_m) \int_{x_m}^{\infty} K_0(x')\, q(x')\, x'\, dx' + K_0(x_m) \int_0^{x_m} I_0(x')\, q(x')x'\, dx'} . \tag{31}$$

Because of $q \propto n_\mathrm{e}$ an iterative procedure, starting e.g. with expression (11) as a first approach on the right hand side, may be needed to obtain a result with the desired accuracy. For a box-like distribution $\hat{q} = (\theta(x - x_1) - \theta(x - x_2))$ an analytical solution can be derived using $\int xK_0(x)\, dx = -xK_1(x)$ and $\int xI_0(x)\, dx = xI_1(x)$. The result reads:

$$n(x) = \frac{1}{N} \begin{cases} I_0(x)\,(x_1K_1(x_1) - x_2K_1(x_2)) & x \le x_1 \\ I_0(x)\,(xK_1(x) - x_2K_1(x_2)) + K_0(x)\,(xI_1(x) - x_1I_1(x_1)) & x_1 < x < x_2 \\ K_0(x)\,(x_2I_1(x_2) - x_1I_1(x_1)) & x \ge x_2 \end{cases} \tag{32}$$

with the normalizing nominator

$$N = I_0(x_m)\,(x_mK_1(x_m) - x_2K_1(x_2)) + K_0(x_m)\,(x_mI_1(x_m) - x_1I_1(x_1)) . \tag{33}$$

The maximum is this time to be determined from

$$x_1I_1(x_1)K_1(x_m) - x_2I_1(x_m)K_1(x_2) = 0 . \tag{34}$$

ACKNOWLEDGEMENT

The support of the PSI-2 group in particular of Dr. W. Bohmeyer and Mrs. M. Baudach is gratefully acknowledged.

REFERENCES

[1] J.B. Taylor. Phys. Fluids, 4(9):1142, 1961.
[2] N. D'Angelo and N. Rynn. Phys. Fluids, 4(10):1303–1306, 1961.
[3] D. Pfirsch and A. Schlueter. IPP-Report: MPI/PA/7, 1962.
[4] L. Spitzer. Phys. Fluids, 3:659, 1960.
[5] F.F. Chen. Introduction to Plasma Physics and Controlled Fusion. Plenum Press, N.Y., London, 1984.
[6] J.W. Connor and H.R. Wilson. Plasma Phys. and Contr. Fusion, 36:719–795, 1994.
[7] A.J. Wootton, B.A. Carreras, H. Matsumoto, K. McGuire, W.A. Peebles, Ch.P. Ritz, P.W. Terry, and S.J. Zweben. Physics of Fluids B, 2(12):2879–2893, 1990.
[8] T.D. Rognlien. Plasma Phys. and Contr. Fusion, 47:A283–A295, 2005.
[9] G.Y. Antar, S.I. Krasheninnikov, P. Devynck, R.P. Doerner, E.M. Hollmann, J.A. Boedo, S.C. Luckhardt, and R.W. Conn. Physical Review Letters, 87(6):065001–1, 2001.

[10] G. Fussmann, W. Bohmeyer, S. Klose, and P. Kornejew. 11th Int. Congr. On Plasma Physics: ICCP 2000, Quebec/Canada, III:744–747, 2000.
[11] O. Waldmann. Plasma shadows in magnetised plasmas. diploma thesis, Humboldt University, Berlin, 2005.
[12] O. Waldmann, B. Koch, and G. Fussmann. AIP Conf. Proc., 812:443–446, 2005.
[13] V.I. Demidov, S.V. Raynskaia, and K. Rypdal. Rev. of Sci. Instr., 73(10):3409–3439, 2002.
[14] O. Jensen. Contr. Plasma Phys., 42(5):526– 536, 2002.
[15] H. Meyer, S. Klose, E. Pasch, and G. Fussmann. Phys. Rev. E, 61(4):4347– 4356, 2000.
[16] G. Fussmann, H. Meyer, and E. Pasch. Contr. Plasma Phys., 36(4):501–517, 1996.
[17] W. Lotz. Zeitschrift für Physik A, 216(3):241–247, 1968.
[18] R.J. Goldston and P.H. Rutherford. Introduction to Plasma Physics. IOP Publishing, Bristol and Philadelphia, 1995.
[19] W.R. Smythe. Static and Dynamic Electricity. McGraw-Hill Book Company, New York, 3rd edition, 1968.
[20] P.C. Stangeby. The Plasma Boundary of Magnetic Fusion Devices. Institute of Physics Publishing, London, 1st edition, 2000.
[21] H. Kastelewicz and G. Fussmann. Contr. Plasma Phys., 44:352–360, 2004.
[22] R. Janev, W. Langer, D. Post, J.R. Evans, and H. Kennet. Elementary processes in hydrogen-helium plasmas: Cross-sections and rate coefficients. Springer-Verlag, N.Y., Berlin, 1987.

[1]MAX-PLANCK-INSTITUT FÜR PLASMAPHYSIK, EURATOM ASSOCIATION, GREIFSWALD, GERMANY
Current address: [1]Lawrence Berkeley National Lab, Berkeley, CA/USA
E-mail address: OWaldmann@lbl.gov

[2]EURATOM/UKAEA FUSION ASSOCIATION, CULHAM SCIENCE CENTRE, ABINGDON, UNITED KINGDOM

[3]INSTITUT FÜR PHYSIK, HUMBOLDT-UNIVERSITÄT ZU BERLIN, GERMANY